Mechanistic Insights into the Structural Asymmetry of the LanFEG Transporter NisFEG in Lantibiotic Immunity

Pablo A. Cea[1], Julia Gottstein[2], Stephan Schott-Verdugo[3], Christian Mammen[2], Sander H.J. Smits[2,4,5], Holger Gohlke[1,3,5]*

[1]Institut for Pharmaceutical and Medicinal Chemistry, Heinrich Heine University Düsseldorf, Düsseldorf, Germany

[2]Institute of Biochemistry, Heinrich Heine University Düsseldorf, Düsseldorf, Germany

[3]Institute of Bio- and Geosciences (IBG-4: Bioinformatics), Forschungszentrum Jülich GmbH, Jülich, Germany

[4]Center for Structural Studies, Heinrich Heine University Düsseldorf, Düsseldorf, Germany

[5]Interfaculty Center for Membrane Research, Heinrich Heine University Düsseldorf, 40225 Düsseldorf, Germany

Keywords: Nisin, NisFEG, LanFEG, lantibiotic, molecular simulations

Running title head: Structural Asymmetry of LanFEG Transporters in Lantibiotic Immunity

* Corresponding author

Tel.: +49-211-81-13662

Email: gohlke@uni-duesseldorf.de

Abstract

Nisin is one of the best studied antimicrobial peptides. Still, how nisin-producing strains can protect themselves against nisin's bactericidal effects is only partially understood. Located within the nisin biosynthesis operon, the heterotetrameric ABC transporter NisFEG transports nisin to the extracellular environment, granting autoimmunity to the producer strain. NisFEG belongs to the LanFEG family of ABC transporters, members of which are found in some lantibiotic-producing bacterial strains. However, their structure has not been elucidated. In this work, we constructed a full atom model of NisFEG in the ATP-bound conformation. The architecture of the complex reveals a narrow contact interface between the two transmembrane chains, with prominent lateral clefts, similar to those observed in other exporters of hydrophobic compounds. Through molecular dynamics (MD) simulations, we observed that one of the most conserved elements of the LanFEG family, the E-loop of the nucleotide-binding domain, interacts preferentially with a small intracellular helix of the NisG transmembrane chain. By combining co-solvent MD simulations and predictions of the binding mode of the terminal segment of nisin, we could identify a putative interaction surface, located predominantly on NisE. Our results suggest that nisin extrusion operates in an asymmetric manner, where contacts between the E-loop and NisG are the driving force for the conformational changes triggered by ATP hydrolysis, whereas the NisE subunit is the main mediator of interactions with the lantibiotic. This functional asymmetry could explain why the LanFEG family has evolved two distinct transmembrane chains, where each one was selected to perform a single step in an optimal way, maximizing the immunity of lantibiotic-producing bacteria.

Introduction

Bacteria produce antimicrobial peptides (AMPs) that target closely related species for survival. These peptides are produced under stress conditions, including limited nutrient availability or nutrient starvation, and are produced by both Gram-(+) and Gram-(-) bacteria and usually possess a narrow-spectrum antibacterial activity. Bacteriocins are a class of AMPs of particular interest since they can exert different modes of action in both genera.

Lanthipeptides are a class of bacteriocins that are produced by specific biosynthetic clusters mainly in Gram-positive bacteria, but their occurrence is not restricted to this group; they are also found in Gram-negative bacteria [1] and cyanobacteria [2, 3]. They are ribosomally synthesized as pre-peptides and undergo several post-translational modifications (PTMs) and are activated after secretion by leader peptide cleavage via a specific protease. The most distinctive PTMs occur on serine and threonine residues that are dehydrated, resulting in the non-standard α,β-unsaturated amino acids 2,3-didehydroaline (Dha) and 2,3-didehydobutyrine (Dhb) [4, 5], followed by a Michael-type condensation of these amino acids with cysteine residues, yielding a thioether crosslink, so-called lanthionine rings (Lan or MeLan rings) [6, 7].

Within the bacteria, lanthipeptide operons are organized as biosynthetic gene clusters (cluster I-V), in which the precursor peptide (LanA) is located with the enzymes for modification, transport (LanT), processing (LanP), and regulation (LanR and LanK). In class I and II, genes for immunity against lanthipeptides can be found for (LanI and or LanFEG) [8]. Here LanI is encoding a lipoprotein, which binds the lanthipeptide, and an ABC transporter LanFEG, which expels the lanthipeptide from the membrane, inhibiting pore formation [8].

The best described lantibiotic is nisin [9], which is naturally produced by several *Lactococcus lactis* strains. It comprises 34 amino acids, which form five lanthionine rings, and has a broad spectrum of activity, inhibiting the growth of Gram-positive and Gram-negative bacteria (Supplementary Figure 1) [10]. Nisin acts as a membrane-targeting peptide and has two main mechanisms of action: I) it can bind to the pyrophosphate groups of Lipid II, which is an essential carrier for bacterial cell wall synthesis, thereby sequestering synthesis and halting cell division, and II), nisin/Lipid II complexes embedded in the bacterial membrane can oligomerize leading to the formation of lethal pores [11]. Hence, nisin has both bacteriostatic and bacteriolytic effects, which makes it a highly potent (activity in the low nM range) antibacterial compound [12].

Due to its high potency, high stability, and broad target membrane spectrum, nisin has important industrial applications. Currently, it is the only bacteriocin approved by the FDA to be used as a food preservative [13]. Moreover, intensive research has been performed to bolster its clinical use, especially against therapy-resistant bacteria such as methicillin-resistant *Staphylococcus aureus* (MRSA) [14].

In their natural environments, bacteria use antibiotic production as a means to eliminate closely related competition from a given niche [15]. It is therefore essential that they possess adequate molecular machinery to protect themselves from the detrimental effects of their own antimicrobial compounds. For this reason, within the nisin biosynthesis operon, there is a set of genes that are responsible for conferring immunity to the producing strain [16]. These genes encode for a membrane-anchored protein (LanI) known as NisI and an ABC transporter (LanFEG) known as NisFEG [17].

NisI is a 27 kDa protein with a membrane anchoring region located at the N-terminus and two extracellular β-barrel domains [18]. Current evidence points toward this protein acting as a nisin binder, preventing its interaction with lipid II [19, 20]. Structural data suggest that the binding of nisin to NisI occurs through a binding cleft located between the two β-barrel domains [18] but the C-terminal domain alone is also capable of interacting with the lantibiotic [19].

NisFEG is an ABC transporter belonging to the LanFEG family [21]. The complex is formed by three protein chains, encoded by the genes *nisF*, *nisE*, and *nisG*. The functional channel is organized as a heterotetrameric structure with stoichiometry 2(F):1(E):1(G). This arrangement places NisFEG within type V of ABC transporters, according to the classification scheme proposed by C. Thomas *et al.* [22]. NisG and NisE constitute the transmembrane region of the transporter, while NisF is intracellularly located and forms a homodimer. The dimer contains the nucleotide-binding domains (NBD) that hydrolyze ATP to drive the activity of the transporter. Experimental work showed that NisFEG, as well as other members of the LanFEG family, such as NukFEG, actively remove the lantibiotic from the cellular membrane of *L. lactis* [21, 23]. Recently, the nisin-like biosynthetic gene clusters have been identified in a widely diverse set of organisms, including human pathogenic strains [24], where the presence of, e.g., the *lanfeg* genes is used for the identification of these clusters in the genomic background.

To date, no 3D structure has been experimentally resolved for any member of the LanFEG family. Therefore, the mechanistic details of how the transporter works remain unknown. So far, the sequence-based analysis combined with homology modeling has revealed the presence of a conserved E-loop in LanF proteins. This region is a variation of the conserved Q loop motif

observed in other ABC transporters and is essential for conferring immunity against nisin, but not for ATP hydrolysis, implying a role in the conformational rearrangements required for effective antibiotic removal [25]. Previous work established that the C-terminus of nisin plays an important role in the recognition between NisFEG and the lantibiotic, as nisin variants lacking the terminal region were still deadly against cells expressing NisFEG [26]. Similarly, nisin variants varying the crucial hinge region in nisin or a natural variant of nisin produced by another strain are less well recognized by NisFEG indicating a certain degree of substrate specificity [27, 28]. This suggested that NisFEG specifically targets the pore formation mode of action, which is mediated by the C-terminus of nisin. However, the lack of structural information on NisFEG, combined with the large size of nisin, has hindered the development of a hypothesis that can explain the function of the transporter.

Here, we constructed a full structural model of the ABC transporter NisFEG in its closed conformation bound to ATP. By using molecular dynamics simulations, we provide first insights into the possible role of the E-loop in the channel's function. Furthermore, by combining co-solvent MD simulations and mutational studies, we were able to identify a putative binding region for nisin.

Results

Architecture of the NisFEG transmembrane domain and full-length model of NisFEG

We constructed a model of the full transporter NisFEG using AlphaFold3. Model quality was assessed through the predicted local distance difference test (pLDDT) and the Ramachandran plot (Supplementary Figure 2). To better interpret the predicted structure, we searched for remotely homologous ABC transporters whose structure-function relationships have been better described, using FoldSeek [31] with NisG as query and the PDB100 [31] as target database. Two bacterial proteins were identified that have transporter functions similar to NisFEG: the exporter of virulent peptides PmtCD from *Staphylococcus aureus* [32] (PDB ID 6XJH) and the O-antigen exporter from *Aquifex aeolicus* [33] (PDB ID 7K2T).

Comparing the generated NisFEG models with the structures of the homologous transporters reveals that the general architecture of the different transmembrane chains (TMB) is conserved. In all cases, the five transmembrane helices within a protein chain have a similar spatial arrangement (Figure 1A). However, the relative orientation of the helices in the oligomeric assembly differs between the two experimentally determined structures. In PDB ID

143 7K2T, the protein-protein interface is formed by the direct contact of helices αT1 and αT5 of
144 each opposing chain, whereas in PDB ID 6XJH, the contact is mostly mediated by the two αT5
145 helices of each chain (Figure 1B). A cross-section, perpendicular to the helices at the center of
146 the membrane, reveals a significantly smaller contact surface area between the protein chains
147 in PDB ID 6XJH than in PDB ID 7K2T (1193.9 $Å^2$ vs. 1384.7 $Å^2$, respectively, assessed by
148 PDBePISA [34]) (Figure 1C). Furthermore, this difference in helical arrangement leads to the
149 presence of a large cleft located between the chains of PDB ID 6XJH. The model of the
150 NisE:NisG assembly has a similar transmembrane arrangement to 6XJH, with αT5 and αT1
151 farther apart from each other, and an interface dominated by the interaction of αT5 of the
152 opposing chains, leading to pronounced lateral clefts. Despite the low sequence identity
153 between NisG and NisE (19.67%, aligned with ClustalW), they are structurally very similar and
154 are arranged symmetrically with respect to one another.

155 *Assessing the functional relevance of the conserved E-loop*

156 The LanFEG family possesses a unique structural element known as the E-loop. The name of
157 the loop derives from a conserved Glu residue at its center. So far, this residue is the only amino
158 acid that has been experimentally shown to be essential for the function of the tetramer, but not
159 for ATP hydrolysis [25]. To investigate the structural role of this residue, we performed
160 microsecond-long all-atom molecular dynamics (MD) simulations of the full NisFEG model
161 with ATP-Mg bound in the NBD domains and embedded in a DMPC membrane bilayer. This
162 membrane composition has been successfully used in experimental *in vitro* characterizations of
163 other ABC transporters from *L. lactis* [36]. The simulations reach a state of low-structural
164 variability after ~200 ns (Supplementary Figure 3).

165 The E-loop is located where the TMB and the NisF subunits meet (Figure 2A). The loop sits
166 close to small intracellular helical segments present in both TMB chains. Here, Glu76 in one
167 of the NisF subunits can form electrostatic interactions with the residues His17, Asn72, and
168 Gln75 located in a short intracellular helix of NisG (hence we will refer to this subunit as $NisF_G$,
169 and the opposite subunit as $NisF_E$), whereas on the other subunit ($NisF_E$), only the residue Gln76
170 is oriented in a way that could potentially interact with the E-loop residue (Figure 2B). As
171 expected, the structural model of the complex shows that the E-loop residue Glu76 does not
172 interact directly with ATP in the nucleotide-bound conformation (Supplementary Figure 4),
173 consistent with the NisF homolog NukF retaining its catalytic activity when the corresponding
174 residue is mutated [25].

175 To evaluate the persistence of interactions mediated by the E-loop residues Glu76, we assessed
176 the presence of hydrogen bonds (defined by a distance cut-off of 3.5 Å and an angle cut-off of
177 135°) between each Glu76 residue and its adjacent TMB residues (Figure 2B, C). The residue
178 Gln76 from NisE does not establish hydrogen bonds with Glu76 $NisF_E$ in any of the replicas.
179 On the other hand, we do observe sporadic, albeit sparse, H-bond formation between Glu76
180 $NisF_G$ with Asn72 and His73, but none with Gln75. We next calculated the distances between
181 the carboxylate group of Glu76 and the functional groups of the interacting residues to
182 determine whether they fall within a range that could still provide electrostatic interactions.
183 From the observed residues, Asn72 stays the closest to Glu76 $NisF_G$, with approximately half
184 of the sampled time spent at distances below 6 Å. It is followed by His73, which has a broad
185 distribution, with significant time spent below 6 Å, but reaching also larger separations. Gln75
186 shows the highest separation to Glu76 from all of the NisG residues, being only surpassed by
187 Gln76 NisE, which spends no time at distances below 6 Å from its possible interaction partner.

188 To further support the functional relevance of the intermolecular interactions formed by
189 Glu76 and the TMB chains, we analyzed the degree of evolutionary conservation of the
190 involved residues. As the E-loop has already been established as a conserved element within
191 LanFEG transporters, we focused on the interaction partners located at the small helical
192 segments of NisG and NisE. To do this, we employed GEMME [37], a program that predicts
193 mutational outcomes by modeling the evolutionary history of sequences through the
194 construction of phylogenetic trees. We hypothesize that if the observed interactions between
195 the intracellular helix of the TMBs and NisF are relevant, they should exhibit greater
196 conservation, and therefore, the GEMME score should reflect this by a higher probability of
197 functional disruption upon mutation. Residues Ala72 and Phe75 are the most conserved on
198 NisE. Both residues point away from $NisF_E$, acting more as hydrophobic contact points to the
199 membrane, while Gln76 has only moderately low scores. On the other hand, Asn72 and Gln75
200 on NisG display low GEMME scores (Figure 3A), indicating that these sites are likely to disrupt
201 protein function if mutated, correlating with their proximity towards Glu76 $NisF_G$.

202 To experimentally corroborate our findings, we mutated the interacting partners of the
203 E-loop (Asn72 and Gln75 in NisG) to alanine. As a control, we also mutated the most prominent
204 and conserved polar residue of the equivalent segment of NisE, Gln76, for which GEMME also
205 predicted a high likelihood of functional alteration upon mutation. The complex variants were
206 expressed in *L. lactis*, and the survivability against nisin was measured. Replacing Gln76 with
207 alanine in NisE does not affect the functioning of NisFEG (Table 1). However, the mutation

208 $NisG_{N72A}$ and $NisG_{Q75A}$ led to a reduction of the base activity of about 25% and 17 %,
209 respectively.

210 To further explore what could be the structural implications of the E-loop-mediated
211 interactions for the system, we calculated a dynamical cross-correlation matrix (DCCM) for the
212 C_α atoms of the whole complex. The DCCM allows us to identify which elements within a
213 protein are moving in a synchronous (correlated) way throughout an MD trajectory [38]. A
214 cross-correlation index equal to 1 indicates that the movement of the atom pair is correlated, an
215 index of -1 indicates that the movement is anti-correlated, and an index of 0 indicates that the
216 movements of the atom pair are independent from one another. Therefore, interactions that are
217 strong enough will cause correlated movements of the interacting elements. Figure 3 shows the
218 cross-correlation indexes for all residues within a radius of 15 Å of Glu76 of each subunit,
219 mapped onto each chain of the complex. The strongest correlations for the first NisF subunit
220 are observed in the short intracellular helix of NisG, where residues Asn72 and Gln75 are
221 located. On the other hand, the correlation index between Glu76 of $NisF_E$ and its equivalent
222 helical segment in NisE is much lower, and stronger correlations occur only within the NBD
223 itself, which further supports that there is no strong interaction between the E-loop in the second
224 NBD and NisE.

225 Additionally, we tested whether the presence of ATP-Mg influences the observed
226 behaviour of the E-loop. For this reason, we constructed an alternative model in the apo state
227 and performed equivalent MD simulations. The model showed slightly lower pLDDT values
228 for the residues at the interface between the transmembrane regions and the NBDs
229 (Supplementary Figure 2), and more structural variation was observed in the latter during the
230 MD simulations (Supplementary Figure 5). Both models show an almost identical conformation
231 ($RMSD_{backbone}$: 0.6 Å, Supplementary Figure 6A). The contacts mediated by the E-loop are also
232 similar, with only a deviation of the rotamer for Asn72 NisG. The apo system shows a similar
233 interaction pattern as the ATP-bound state, with more H-bonds between NisG and $NisF_G$
234 observed than between NisE and $NisF_E$ (Supplementary Figure 6B). However, in two of the
235 MD replicas, sporadic contacts to Gln76 from NisE occur, while Asn72 NisG does not interact
236 directly with the E-loop. Overall, only slight deviations between the two models are observed.

237 Lastly, we checked whether the E-loop could also establish contacts relevant for
238 oligomerization between the NBDs. Here, we identified Lys129 on NisF with the potential to
239 form an electrostatic interaction with Glu76 of the opposing NisF subunit (Supplementary
240 Figure 7A). The interaction is very dynamic, with the distance between both residues oscillating

241 between 4 and 10 Å, without a noticeable asymmetry between chains. To assess its importance,
242 we mutated Lys129 to alanine, which results in an activity reduction of 36% (Table 1).

243 Together, these results show that the E-loop is an asymmetric interface element that
244 directly interacts with NisG but does not display the same interaction pattern with NisE.

245 Co-solvent MD simulations to identify putative regions in NisFEG interacting with nisin

246 So far, there is no evidence on where and how NisFEG binds to nisin. To generate a
247 hypothesis of where the binding interface might be located, we employed cosolvent MD
248 simulations [39]. In this technique, small molecule probes that mimic the main chemical
249 moieties of a ligand are placed in the simulation box and allowed to freely diffuse and interact
250 with the protein surface. Since ligand binding sites provide a chemical environment favorable
251 for non-covalent interactions, the small probes will accumulate in them. This technique has
252 been proven effective to identify previously uncharacterized orthosteric and allosteric sites [39,
253 40]. Since nisin is a highly hydrophobic molecule and rich in peptide bonds, we utilized
254 benzene, *N*-methylacetamide, acetone, and methanol as probes (Figure 5A). We performed five
255 independent simulation replicas of 1 μs length per probe in the same explicit membrane used
256 above, and then analyzed in which regions of the complex the accumulation of the different
257 probes overlapped. The convergence of the simulation results was assessed by monitoring the
258 radial distribution function of each probe, setting a mask for all the heavy atoms of the probes
259 and the backbone atoms of the protein, and by inspecting the change of normalized density
260 pattern over the simulation course (Supplementary Figure 8).

261 Overall, NisFEG accumulates more probes at its transmembrane region than at its
262 intracellular domains. We could identify four regions where there is a marked simultaneous
263 colocalization of at least three probes. The first and largest one (Site I) is located at the
264 extracellular face of the transporter, right at the cleft between NisE and NisG. This site shows
265 a high affinity for the backbone mimetic probes, with minor densities for both the polar and
266 hydrophobic probes. The second site (Site II) is smaller, located on the external side of NisG.
267 The last two sites (Site III and IV) are situated within the lateral clefts of the transporter, one at
268 each side. Site III is slightly smaller and located within the helices of NisE. Interestingly,
269 between this site and Site I, we observe a small accumulation of acetone and benzene. Site IV
270 is larger, with a broader affinity for methanol. These results show that the transmembrane
271 surface of NisFEG has sites with the right physicochemical properties that could possibly form
272 interactions with a peptidic ligand.

Modeling the interaction between NisFEG and the C-terminus of nisin

Previous work has demonstrated that upon removal of the C-terminus of nisin (C-Nis), NisFEG can not protect the cell against it, implying a direct interaction between the transporter and this part of the lantibiotic [26]. Given that (C-Nis) comprises only six residues (Supplementary Figure 1), current ML-based predictors for biomolecular interactions could infer a possible binding mode. We therefore used Boltz-2 to predict the structure of the full NisFEG complex in the presence of C-Nis. To ensure a proper sampling of the conformational solution space, we generated 600 structural models of the full system.

To infer a putative binding mode, we first clustered the generated poses to identify whether there are clear trends within the data. Since C-Nis is a peptide with a high number of degrees of freedom, clustering only by ligand RMSD can result in significant information loss; thus, we used the coordinates of each ligand's atom and performed a dimensionality reduction through t-distributed Stochastic Neighbor Embedding (t-SNE). t-SNE generates a nonlinear embedding optimized to preserve local neighborhood relationships of multidimensional data. The distribution of each possible C-Nis configuration on the t-SNE projection space is shown in Figure 6A. There, data points were additionally clustered by their proximity using a Gaussian mixture model and colored accordingly. All the sampled solutions converge to the same location of the NisFEG complex, which is on the extracellular face of the cleft formed by the interface of the transmembrane subunits NisE:NisG. The data is divided into two large clusters, i) and ii), which represent the two possible N- to C-terminus orientations that the lantibiotic could adopt (Figure 6B), of which group ii) occurs 2.8 times more frequently. From this main orientation, we identified the three largest subclusters with 84, 71, and 68 poses, respectively. The subclusters are cohesive groups of poses with average pairwise RMSD values below 3.3 Å each.

From these subclusters, we selected the pose corresponding to the medoid of the projections as representative to analyze in detail the binding mode, showing the interacting amino acid residues within 5 Å of C-Nis (Figure 7). In all of the observed poses, we observe a larger proportion of residues of NisE surrounding the ligand than of NisG. Furthermore, the position of the His residue of C-Nis is conserved in the three clusters, being flanked by the aromatic residues $Phe172_{NisE}$, $W48_{NisE}$, and $Y47_{NisE}$. Also of note, in all of the clusters, the N-terminus of the peptide, which would represent where the rest of the nisin molecule would be attached, is placed in an exposed position at the edge of the NisE:NisG interface, implying that the rest of the molecule might fit onto one of the lateral clefts of the transporter. Coincidentally,

306 in poses from group ii), the N-terminus position would leave the rest of the nisin molecule
307 pointing towards where the previously observed Site III on NisE was observed.

308

309 **Discussion**

310 In this work, we constructed a full model of the lantibiotic transporter NisFEG from *L.*
311 *lactis* and focused our analysis on two unknown aspects of it: what is the role of the conserved
312 E-loop, and where could the putative binding site of nisin be located.

313 A structure-based search using NisG as the query allowed us to identify a distant
314 homolog that also exports a highly lipophilic membrane-disrupting peptide, the ABC
315 transporter PmtCD; a sequence-based search would not have allowed us to identify the homolog
316 due to a sequence identity of only 15.5%. In both cases, the architecture of the transmembrane
317 region of the complex follows a similar arrangement, resulting in a narrow interface with
318 prominent clefts at the sides. Zeytuni *et al.* highlighted the possibility that these side clefts could
319 serve as binding sites for the target peptide [32]. This is a reasonable hypothesis given that the
320 substrate of PmtCD is a hydrophobic helical peptide that embeds itself within the lipid bilayer.
321 This makes the conventional inward-open cavity commonly observed in other ABC transporters
322 for soluble substrates unnecessary, since the peptide cargo already resides in the membrane.
323 Furthermore, eukaryotic ABC transporters that export large hydrophobic substances, such as
324 the ABCA1 transporter, also display a narrow interface mediated mostly by a single helix and
325 large lateral surface clefts [41]. Moreover, the cryo-EM structure of this distantly homologous
326 transporter revealed lipid-like densities at the lateral clefts. It has also been proposed that other
327 ABC transporters, including ABCB4, can function as phospholipid floppases through
328 interactions mediated by the lateral helices [42]. Overall, the current knowledge on ABC
329 transporters suggests that whenever hydrophobic substrates need to be translocated, they can
330 be transported directly from the membrane through interactions with the side of the protein.
331 Thus, it is likely that the whole LanFEG family might follow a similar mechanism.

332 One aspect that makes transporters of the LanFEG family different from other members
333 of the type V class of ABC transporters is the presence of two distinct transmembrane chains
334 instead of a homodimeric transmembrane region. NisG and NisE share a low sequence identity
335 of 20%, but the heterodimer is required for a functional transporter, suggesting that natural
336 selection has led to the divergence of the two chains. Interestingly, our MD simulations revealed
337 that one of the most conserved elements of the LanFEG family, the E-loop of the NBD, interacts

differentially with either transmembrane subunit, even though there are two copies of the loop at equivalent positions within the complex. The E-loop is located near a short intracellular helix present in both transmembrane subunits, but only NisG forms direct polar contacts with the central Glu76 of the E-loop. Furthermore, the helical residues of NisG are more conserved than the equivalent positions of NisE. These conserved interactions apparently have a structural effect: the coupling of motions between the E-loop of $NisF_G$ and NisG. Given that E76 is essential for the channel function, the E-loop element likely plays a key role in the propagation of conformational rearrangements triggered by the hydrolysis of ATP towards the transmembrane region that are required for effective nisin removal, thus playing a similar role as the Q-loop in other ABC transporters [43]. Furthermore, experimental work on the human multidrug resistance transporter ABCB1 has shown functional redundancy in the Q-loop; if only one chain is mutated, the transporter retains its activity [44]. This means that it would be feasible for LanFEG transporters to function relying on a single half of the complex to power the required conformational rearrangements. However, the precise nature and extent of conformational rearrangements occurring at the transmembrane region remain open questions within the LanFEG family.

Furthermore, we also explored the influence that ATP binding might exert on the structure of NisFEG. In other ABC transporters, the equivalent loop, known as the Q-loop, has also been proposed to play a role in nucleotide sensing by interacting with the γ-phosphate [45]. Modelling of NisFEG in the apo and ATP-bound states revealed no significant reorientations of the E-loop; however, it is critical to point out that deep learning-based structure prediction methods are limited in predicting the conformational diversity of mobile proteins [46]. Even though we see some slight changes in hydrogen bond patterns between the TMB and the E-loop in the apo model, the residues involved also have a lower pLDDT score, and therefore lower confidence in the accuracy of the model, meaning that the differences could also just be a byproduct of modelling inaccuracies and not a real effect caused by the ATP.

The lack of structural information for LanFEG transporters, combined with the large size and complexity of nisin, has hindered the proposal of a putative binding mode. Our first step to uncover a possible nisin-binding region within NisFEG was to conduct co-solvent MD simulations with probes that mimic the main features of nisin, an approach that has been successfully applied to identify unknown ligand binding sites [47]. Our results showed a significantly larger and more varied accumulation of probes within the transmembrane region, with a main site located at the extracellular interface of NisE with NisG, two sites located at the lateral clefts of the transporter, and one minor peripheral site on NisG. Based on the size of the

372 sites, it is likely that the minor site II is not relevant for nisin interaction, while the other sites
373 (Site I, III, and IV) are more likely to provide a marked interaction surface for a peptide the size
374 of nisin.

375 The results derived from co-solvent MD simulations paint a broader and clearer picture
376 when seen together with the structural prediction of the binding mode of C-Nis. In the latter, all
377 the runs resulted in the peptide being placed on the extracellular face of the interface between
378 NisE and NisG, perfectly matching site I, which was mostly defined by its preference for the
379 backbone mimicking probes (acetone and N-acetamide), supporting the idea that this could
380 indeed be a functionally relevant site, optimized to interact with linear peptides. On this site,
381 the two possible N-to-C orientations along the cleft were observed, but one was 2.8-fold more
382 frequently sampled. This opens the possibility that the rest of the molecule rests in one of the
383 lateral clefts, which have been speculated to be relevant in other peptide-transporting ABC
384 transporters [31], and would agree with either of the lateral sites observed in the co-solvent
385 simulations. The most populated configuration of C-Nis leaves the N-terminus, and therefore
386 the rest of the nisin, in a position where it would be possible to interact with site III. Although
387 this site is smaller than site IV, a small density of acetone and benzene is present, possibly
388 bridging site III to the larger site I, allowing it to form a cohesive binding interface spanning
389 from the top of the transporter to its lateral cleft.

390 This putative binding interface makes sense in light of the experimental data regarding how
391 both nisin and NisFEG work. Structural studies of the mechanism of action of nisin have shown
392 that the lanthionine rings A, B, and C form a cage surrounding the target molecule, lipid II,
393 whereas the C-terminus of the molecule remains flexible, connected by a hinge region, and is
394 later involved in the formation of bacteriolytic pores [48]. Mutational analysis of nisin variants
395 has shown that both the last six amino acids and the last lanthionine rings D/E are required for
396 NisFEG to effectively protect the cells [26], implying that there must be a direct association
397 between the transporters and these regions of nisin. Since these elements are not bound to lipid
398 II and remain highly flexible, there is a higher likelihood of encountering and binding to
399 NisFEG, thus initiating the first step for extrusion from the membrane. Therefore, these two
400 essential regions, the C-terminus and the last rings, might bind to the identified Sites I and III,
401 respectively.

402 A more detailed analysis of the putative binding modes of C-Nis reveals that, even though
403 the peptide sits at the middle of both NisG and NisE, the interaction is asymmetric, with more
404 residues from NisE in close contact to the peptide. His31 of the C-terminus is surrounded by

405 aromatic residues from NisE, a result that is consistent across the three largest binding mode
406 clusters. As previously mentioned, all of the binding modes assessed would position the rest of
407 nisin in a position to make interactions with site III, which is also located solely in NisE. This
408 reinforces the asymmetry of function observed for the transmembrane chains. On the one hand,
409 only NisG showed the capacity of forming interactions with the E-loop, on the other hand, NisE
410 seems to dominate the putative interactions with nisin, suggesting that there might be a
411 specialization of roles for each transmembrane chain.. This functional asymmetry could provide
412 an interesting explanation of why there is such a low sequence identity between NisG and NisE;
413 evolution has optimized each chain to perform a specific part of the nisin removal process.
414 Heteromeric complexes formed by homologous chains with low identity are relatively
415 common. For instance, heterodimeric and heterotretrameric ABC transporters are often found
416 in eukaryotic cells, where subunit heterogeneity has been proposed as a means for regulating
417 and fine-tuning the function of the complex [49, 50]. Because the efficacy of a lantibiotic is
418 inherently constrained by the capacity of the producing cell to withstand the toxicity of its own
419 product, there is a strong purging, selective pressure driving the optimization of the immunity-
420 related proteins. Therefore, fine-tuning each transmembrane subunit to drive a specific part of
421 the process could be a favorable evolutionary adaptation.

422 It is important to note that the large surface and hydrophobic nature of the putative contacts
423 between NisE and NisG make it difficult to experimentally probe the sites, since probably the
424 binding is driven by the sum of the interactions rather than dominated by single residues. Thus,
425 mutational assays might not give conclusive data, and any effect on transporter activity might
426 be confounded with other issues, such as stability and membrane translocation.

427 Taken together, our results represent the first step in constructing a structural hypothesis of
428 how the LanFEG family of ABC transporters, and more specifically NisFEG, confer immunity
429 to lantibiotic-producing bacterial strains. This mechanism of action is summarized in Figure 8.
430 Nisin, initially bound to lipid II, has its C-terminus free and exposed, which can be recognized
431 by the sites present on NisE. Then, ATP hydrolysis powers conformational changes that are
432 transmitted through the E-loop – NisG association toward the rest of the transporter and enable
433 the removal of nisin from the membrane.

434

435

Materials and Methods

Modeling of NisFEG

A structural model of the transmembrane region involving the protein chains NisE (NCBI: WP_014570414.1) and NisG (NCBI: WP_017864242.1) and NisF in the presence of ATP-Mg was generated using AlphaFold3. The quality of the models was assessed by the metrics of pLDDT and PAE, and by stereochemical analysis with a Ramachandran plot (generated using: https://github.com/Joseph-Ellaway/Ramachandran_Plotter).

The search for further homologous proteins was performed using the FoldSeek [31] webserver with default parameters and the best resulting NisE and NisG models generated by AlphaFold3 as input. The structure of the PmtCD transporter (PDB ID 6XJH) was used as a template for further modeling of the whole complex.

Conventional and cosolvent all-atom molecular dynamics simulations.

The protonation state of the protein was assigned using Propka in Schrödinger [61]. The model was embedded in a DMPC membrane bilayer using PACKMOL-Memgen [62] and TIP3P as the water model. The orientation of the protein within the membrane was previously determined using the OPM-PPM webserver [58]. Topology and coordinates files were generated using tleap [63]. The forcefield ff19SB [64] was used for the protein and lipid17 [65] for the membrane. The parameters for ATP-Mg were taken from the Bryce database [66, 67]. Counterions were added to maintain the electroneutrality of the system. All simulation work was performed using Amber22 [68]. The total system contained 139,261 atoms, made out 31,616 water molecules. 315 lipids, and 33 ions. The initial minimization of the system was performed by adapting the protocol from Roe & Brooks [69], consisting of a total of twelve individual stages. First, 5000 steps of steepest descent minimization followed by 15000 steps of conjugated gradient minimization with positional restraints with a force constant of 5 kcal mol^{-1} $Å^{-2}$ placed on all solute atoms was carried out. Then, the system was heated from 0 to 300 K in an NVT ensemble in a window of 20 ps with a time step of 1 fs, using a Langevin thermostat [70] with a gamma coefficient of 1 ps^{-1}, keeping the same restraints in place. Then three successive minimizations of 1000 steps of steepest descent were performed, reducing the restraints on the solute atoms to 2, 0.1, and 0 kcal mol^{-1} $Å^{-2}$. Afterward, an NPT run of 300 ps with a time step of 1 fs was performed, using an anisotropic Monte-Carlo barostat with a pressure relaxation time of 2 ps and a constant temperature of 300 K with a restraint of 1 kcal mol^{-1} $Å^{-2}$ over solute atoms,

468 followed by another identical run but with a lower restraint of 0.8 kcal mol^{-1} $Å^{-2}$. Five
469 subsequent NPT runs of the same length and time steps were performed, placing the restraints
470 only on the protein atoms and decreasing the force constant by 0.2 kcal mol^{-1} $Å^{-2}$ in each run
471 until reaching 0 kcal mol^{-1} $Å^{-2}$. Production runs were performed for 1 μs with a time step of 2
472 fs using the GPU-accelerated implementation of pmemd [71]. The first 10 ns of production
473 were run with a positional restraint of 0.1 kcal mol^{-1} $Å^{-2}$ on protein atoms and a width of the
474 non-bonded skin of 5 Å and discarded from further analysis. Five independent replicas were
475 carried out saving the coordinates of the system every 100 ps. All simulations were performed
476 using the SHAKE algorithm [72] to constrain the length of bonds to hydrogens and a non-
477 bonded cut-off of 10 Å.

478 Distances between residues throughout the simulations were calculated using the *distance*
479 command in cpptraj [73]. The distances were calculated between the centre of mass of the
480 carboxylic oxygens of Glu76 and the centre of mass of nitrogen and oxygen of the amide group
481 from either Asn72 or Gln75, or the sidechain nitrogen from Lys129. A per-residue cross-
482 correlation matrix was calculated using the *matrix* command in cpptraj. To suppress spurious
483 correlations, we used only the 80% of the total frames with the lowest RMSD with respect to
484 the starting configuration,

485 For cosolvent MD simulations, the systems were prepared using acetone, benzene, methanol,
486 or *N*-methylacetamide as a probe. The placement of the probe molecules was performed using
487 PACKMOL-Memgen in a ratio of 1 molecule of co-solvent per 99 molecules of water, using
488 the same membrane and solvent as described previously. The parameters for each co-solvent
489 are included within PACKMOL-Memgen [62]. Five independently packed systems were
490 generated for each probe to randomize the initial position of the probes. The same minimization,
491 thermalization, and pressurization protocol as previously described was used. Five independent
492 production replicas per random packing were carried out, utilizing the same conditions as
493 previously described, but with a production run length of 500 ns. The density distributions for
494 each probe were calculated by first aligning the backbone atoms of the protein using the *rms*
495 command in cpptraj and wrapping the solvent and cosolvent molecules with the *autoimage*
496 function. Densities were calculated using the *volmap* tool of VMD [74] with a resolution of 1 Å
497 and an atom size of 3 Å. To assess the convergence of the cosolvent sampling, the density
498 calculation was repeated at different total simulation times to ensure the invariance of the
499 density distribution. Also, the radial distribution function for each probe was calculated against
500 the Cα atoms of the protein in a window of 100 Å, using the *radial* command on cpptraj [73],
501 ignoring intramolecular interactions.

502 **Modeling of NisFEG bound to C-Nis**

503 Models of the full NisFEG complex in the presence of ATP-Mg and the last six amino acids of
504 nisin were generated using Boltz-2 [76]. 600 independent runs were performed, with 20 recycle
505 steps. Data processing was carried out using SciPy in Python.

506 **Site-directed mutagenesis, protein expression, and measurement of NisFEG activity**

507 NisE, NisG, and NisF (or the inactive variant $NisF_{H181A}$, to generate a sensitive control) were
508 cloned into a pILSV shuttle vector as previously described elsewhere [26]. Site-directed
509 mutagenesis was performed by PCR using Phusion DNA polymerase, the template NisFEG-
510 pILSV vector, and a mutagenic primer pair (Table 2). The mutated plasmids were transformed
511 into *L. lactis* NZ9000 by electroporation at 1 kV, 25 µF, 5.0 msec.

512 Nisin was purified and quantified as described elsewhere [77]. The transformed *L. lactis* strains
513 harbouring either the WT or a variant were grown overnight in GM17 media supplemented with
514 10 µg / mL chloramphenicol in the presence of 1 ng / mL of nisin for inducing expression. The
515 next day, the cells were diluted to an OD_{600} of 0.1 in fresh GM17 media and incubated for 30
516 minutes at 30 °C. Then, 150 µL of bacterial sample were loaded into a 96-well plate alongside
517 50 µL of nisin solution. The samples were incubated for 5-7 hours at 30°C, and the OD_{600} was
518 measured. The activities of NisFEG, control strain, and mutants were calculated as described
519 in previous work [71].

520

ASSOCIATED CONTENT

Supporting Information

Supporting Information is available free of charge at: [XXX: Add link to paper.]

Additional simulation data shown in supplementary figures and supplementary references (PDF).

AUTHOR INFORMATION

Corresponding Authors

H.G.:

Address: Universitätsstr. 1, 40225 Düsseldorf, Germany.

Phone: (+49) 211 81 13662

E-mail: gohlke@uni-duesseldorf.de

ORCID

Holger Gohlke: 0000-0001-8613-1447

Author Contributions

Conceptualization, PAC, HG; methodology, PAC, SS-V (modeling and simulations) & JG, CM (biochemistry); writing - original draft preparation, PAC, HG; writing - review and editing, JG, CM, SHJS; data analysis and interpretation, PAC, JG, SHJS, HG; supervision and project administration, SHJS, HG; funding acquisition, SHJS, HG. All authors have read and agreed to the published version of the manuscript.

Funding Sources

This research was funded by grants from the Deutsche Forschungsgemeinschaft [DFG, German Research Foundation; 270650915/GRK 2158 (to HG, SHJS)]. The Center for Structural Studies is funded by the Deutsche Forschungsgemeinschaft [DFG; 417919780 (to SHJS)] and is part of StrukturaLink Rhein-Ruhr, which is funded by the Deutsche Forschungsgemeinschaft [DFG; 573727698].

Notes

The authors declare no competing financial interest.

Acknowledgements

We are grateful for computational support and infrastructure provided by the "Zentrum für Informations- und Medientechnologie" (ZIM) at the Heinrich Heine University Düsseldorf and the computing time provided by the John von Neumann Institute for Computing (NIC) to HG on the supercomputer JUWELS at Jülich Supercomputing Centre (JSC) (user ID: VSK33). We thank Martina Wesemann from the Institute of Biochemistry for excellent support.

DATA AND SOFTWARE AVAILABILITY STATEMENT

The software used for generating the models is in the public domain. The Schrödinger software is available here: https://www.schrodinger.com/ . The AMBER package of molecular simulation codes is available here: https://ambermd.org/ . Source data, input files, and processing scripts are available at https://researchdata.hhu.de .

562 **References**

563 1. Goto, Y., et al., *Discovery of unique lanthionine synthetases reveals new mechanistic and*
564 *evolutionary insights.* PLoS Biol, 2010. **8**(3): p. e1000339.
565 2. Tracanna, V., et al., *Mining prokaryotes for antimicrobial compounds: from diversity to*
566 *function.* FEMS Microbiol Rev, 2017. **41**(3): p. 417-429.
567 3. Li, B., et al., *Catalytic promiscuity in the biosynthesis of cyclic peptide secondary metabolites*
568 *in planktonic marine cyanobacteria.* Proc Natl Acad Sci U S A, 2010. **107**(23): p. 10430-5.
569 4. Gross, E. and J.L. Morell, *The presence of dehydroalanine in the antibiotic nisin and its*
570 *relationship to activity.* J Am Chem Soc, 1967. **89**(11): p. 2791-2.
571 5. Gross, E. and J.L. Morell, *The number and nature of alpha,beta-unsaturated amino acids in*
572 *nisin.* FEBS Lett, 1968. **2**(1): p. 61-64.
573 6. Li, B., et al., *Structure and Mechanism of the Lantibiotic Cyclase Involved in Nisin Biosynthesis.*
574 Science, 2006. **311**(5766): p. 1464-1467.
575 7. Negash, A.W. and B.A. Tsehai, *Current Applications of Bacteriocin.* Int J Microbiol, 2020.
576 **2020**: p. 4374891.
577 8. Smits, S.H.J., L. Schmitt, and K. Beis, *Self-immunity to antibacterial peptides by ABC*
578 *transporters.* FEBS Lett., 2020. **594**(23): p. 3920-3942.
579 9. Willey, J.M. and W.A.v.d. Donk, *Lantibiotics: Peptides of Diverse Structure and Function.*
580 Annu. Rev. Microbiol., 2007. **61**(1): p. 477-501.
581 10. Cheigh, C.-I. and Y.-R. Pyun, *Nisin Biosynthesis and its Properties.* Biotechnol. Lett., 2005.
582 **27**(21): p. 1641-1648.
583 11. Medeiros-Silva, J., et al., *High-resolution NMR studies of antibiotics in cellular membranes.*
584 Nat. Commun., 2018. **9**(1): p. 3963.
585 12. Wiedemann, I., et al., *Specific Binding of Nisin to the Peptidoglycan Precursor Lipid II*
586 *Combines Pore Formation and Inhibition of Cell Wall Biosynthesis for Potent Antibiotic*
587 *Activity* *. J. Biol. Chem., 2001. **276**(3): p. 1772-1779.
588 13. Gharsallaoui, A., et al., *Nisin as a Food Preservative: Part 1: Physicochemical Properties,*
589 *Antimicrobial Activity, and Main Uses.* Crit. Rev. Food Sci. Nutr., 2016. **56**(8): p. 1262-1274.
590 14. Cotter, P.D., C. Hill, and R.P. Ross, *Bacterial lantibiotics: strategies to improve therapeutic*
591 *potential.* Curr Protein Pept Sci, 2005. **6**(1): p. 61-75.
592 15. Stubbendieck, R.M. and P.D. Straight, *Multifaceted Interfaces of Bacterial Competition.* J
593 Bacteriol, 2016. **198**(16): p. 2145-55.
594 16. Siegers, K. and K.D. Entian, *Genes involved in immunity to the lantibiotic nisin produced by*
595 *Lactococcus lactis 6F3.* Applied and Environmental Microbiology, 1995. **61**(3): p. 1082-1089.
596 17. Stein, T., et al., *Function of Lactococcus lactis Nisin Immunity Genes nisI and nisFEG after*
597 *Coordinated Expression in the Surrogate Host Bacillus subtilis.* J. Biol. Chem., 2003. **278**(1):
598 p. 89-94.
599 18. Jeong, J.H. and S.C. Ha, *Crystal Structure of NisI in a Lipid-Free Form, the Nisin Immunity*
600 *Protein, from Lactococcus lactis.* Antimicrob Agents Chemother, 2018. **62**(3).
601 19. Hacker, C., et al., *The Solution Structure of the Lantibiotic Immunity Protein NisI and Its*
602 *Interactions with Nisin.* J Biol Chem, 2015. **290**(48): p. 28869-86.
603 20. Takala, T.M., et al., *Lipid-free NisI: interaction with nisin and contribution to nisin immunity*
604 *via secretion.* FEMS Microbiol. Lett., 2004. **237**(1): p. 171-177.
605 21. Alkhatib, Z., et al., *Lantibiotics: How do producers become self-protected?* J. Biotechnol., 2012.
606 **159**(3): p. 145-154.
607 22. Thomas, C., et al., *Structural and functional diversity calls for a new classification of ABC*
608 *transporters.* FEBS Lett., 2020. **594**(23): p. 3767-3775.
609 23. Okuda, K., et al., *Cooperative transport between NukFEG and NukH in immunity against the*
610 *lantibiotic nukacin ISK-1 produced by Staphylococcus warneri ISK-1.* J Bacteriol, 2008. **190**(1):
611 p. 356-62.
612 24. Hourigan, D., et al., *Nisin-like biosynthetic gene clusters are widely distributed across*
613 *microbiomes.* mBio, 2025: p. e0154525.
614 25. Okuda, K., et al., *Functional significance of the E loop, a novel motif conserved in the lantibiotic*
615 *immunity ATP-binding cassette transport systems.* J Bacteriol, 2010. **192**(11): p. 2801-8.

26. AlKhatib, Z., et al., *The C-terminus of nisin is important for the ABC transporter NisFEG to confer immunity in Lactococcus lactis.* Microbiologyopen, 2014. **3**(5): p. 752-763.
27. Reiners, J., et al., *Insights in the Antimicrobial Potential of the Natural Nisin Variant Nisin H.* Front Microbiol, 2020. **11**: p. 573614.
28. Zaschke-Kriesche, J., et al., *Influence of nisin hinge-region variants on lantibiotic immunity and resistance proteins.* Bioorg Med Chem, 2019. **27**(17): p. 3947-3953.
29. Baek, M., et al., *Accurate prediction of protein structures and interactions using a three-track neural network.* Science, 2021. **373**(6557): p. 871-876.
30. Mulnaes, D. and H. Gohlke, *TopScore: Using Deep Neural Networks and Large Diverse Data Sets for Accurate Protein Model Quality Assessment.* J. Chem. Theory Comput., 2018. **14**(11): p. 6117-6126.
31. van Kempen, M., et al., *Fast and accurate protein structure search with Foldseek.* Nat Biotechnol, 2024. **42**(2): p. 243-246.
32. Zeytuni, N., et al., *Structural insight into the Staphylococcus aureus ATP-driven exporter of virulent peptide toxins.* Sci Adv, 2020. **6**(40).
33. Caffalette, C.A. and J. Zimmer, *Cryo-EM structure of the full-length WzmWzt ABC transporter required for lipid-linked O antigen transport.* Proc Natl Acad Sci U S A, 2021. **118**(1).
34. Krissinel, E. and K. Henrick, *Inference of macromolecular assemblies from crystalline state.* J Mol Biol, 2007. **372**(3): p. 774-97.
35. Song, Y., et al., *High-resolution comparative modeling with RosettaCM.* Structure, 2013. **21**(10): p. 1735-42.
36. Siarheyeva, A., J.J. Lopez, and C. Glaubitz, *Localization of Multidrug Transporter Substrates within Model Membranes.* Biochemistry, 2006. **45**(19): p. 6203-6211.
37. Laine, E., Y. Karami, and A. Carbone, *GEMME: A Simple and Fast Global Epistatic Model Predicting Mutational Effects.* Molecular Biology and Evolution, 2019. **36**(11): p. 2604-2619.
38. Yu, H. and P.A. Dalby, *A beginner's guide to molecular dynamics simulations and the identification of cross-correlation networks for enzyme engineering.* Methods Enzymol, 2020. **643**: p. 15-49.
39. DasGupta, D., et al., *Identifying Potential Ligand Binding Sites on Glycogen Synthase Kinase 3 Using Atomistic Cosolvent Simulations.* ACS Appl Bio Mater, 2024. **7**(2): p. 588-595.
40. Ghanakota, P. and H.A. Carlson, *Moving Beyond Active-Site Detection: MixMD Applied to Allosteric Systems.* J Phys Chem B, 2016. **120**(33): p. 8685-95.
41. Qian, H., et al., *Structure of the Human Lipid Exporter ABCA1.* Cell, 2017. **169**(7): p. 1228-1239.e10.
42. Prescher, M., et al., *Evidence for a credit-card-swipe mechanism in the human PC floppase ABCB4.* Structure, 2021. **29**(10): p. 1144-1155.e5.
43. Wilkens, S., *Structure and mechanism of ABC transporters.* F1000Prime Rep, 2015. **7**: p. 14.
44. Zolnerciks, J.K., et al., *The Q loops of the human multidrug resistance transporter ABCB1 are necessary to couple drug binding to the ATP catalytic cycle.* Faseb j, 2014. **28**(10): p. 4335-46.
45. Yuan, Y.R., et al., *The crystal structure of the MJ0796 ATP-binding cassette. Implications for the structural consequences of ATP hydrolysis in the active site of an ABC transporter.* (0021-9258 (Print)).
46. Saldaño, T., et al., *Impact of protein conformational diversity on AlphaFold predictions.* Bioinformatics, 2022. **38**(10): p. 2742-2748.
47. Arcon, J.P., et al., *Molecular Dynamics in Mixed Solvents Reveals Protein-Ligand Interactions, Improves Docking, and Allows Accurate Binding Free Energy Predictions.* J Chem Inf Model, 2017. **57**(4): p. 846-863.
48. Hsu, S.-T.D., et al., *The nisin–lipid II complex reveals a pyrophosphate cage that provides a blueprint for novel antibiotics.* Nature Structural & Molecular Biology, 2004. **11**(10): p. 963-967.
49. Sudha, G., N. Naveenkumar, and N. Srinivasan, *Evolutionary and structural analyses of heterodimeric proteins composed of subunits with same fold.* Proteins, 2015. **83**(10): p. 1766-86.
50. Hillebrand, M., et al., *Live cell FRET microscopy: homo- and heterodimerization of two human peroxisomal ABC transporters, the adrenoleukodystrophy protein (ALDP, ABCD1) and PMP70 (ABCD3).* J Biol Chem, 2007. **282**(37): p. 26997-27005.

51. Abrusan, G. and J.A. Marsh, *Ligand Binding Site Structure Influences the Evolution of Protein Complex Function and Topology.* Cell Rep, 2018. **22**(12): p. 3265-3276.
52. Remmert, M., et al., *HHblits: lightning-fast iterative protein sequence searching by HMM-HMM alignment.* Nat Methods, 2011. **9**(2): p. 173-5.
53. Mirdita, M., et al., *ColabFold: making protein folding accessible to all.* Nat Methods, 2022. **19**(6): p. 679-682.
54. Bawono, P. and J. Heringa, *PRALINE: a versatile multiple sequence alignment toolkit.* Methods Mol Biol, 2014. **1079**: p. 245-62.
55. McGuffin, L.J., K. Bryson, and D.T. Jones, *The PSIPRED protein structure prediction server.* Bioinformatics, 2000. **16**(4): p. 404-5.
56. Tusnady, G.E. and I. Simon, *The HMMTOP transmembrane topology prediction server.* Bioinformatics, 2001. **17**(9): p. 849-50.
57. Kallberg, M., et al., *RaptorX server: a resource for template-based protein structure modeling.* Methods Mol Biol, 2014. **1137**: p. 17-27.
58. Lomize, M.A., et al., *OPM database and PPM web server: resources for positioning of proteins in membranes.* Nucleic Acids Res, 2012. **40**(Database issue): p. D370-6.
59. Fleishman, S.J., et al., *RosettaScripts: a scripting language interface to the Rosetta macromolecular modeling suite.* PLoS One, 2011. **6**(6): p. e20161.
60. Studer, G., M. Biasini, and T. Schwede, *Assessing the local structural quality of transmembrane protein models using statistical potentials (QMEANBrane).* Bioinformatics, 2014. **30**(17): p. i505-i511.
61. Olsson, M.H., et al., *PROPKA3: Consistent Treatment of Internal and Surface Residues in Empirical pKa Predictions.* J Chem Theory Comput, 2011. **7**(2): p. 525-37.
62. Schott-Verdugo, S. and H. Gohlke, *PACKMOL-Memgen: A Simple-To-Use, Generalized Workflow for Membrane-Protein-Lipid-Bilayer System Building.* J Chem Inf Model, 2019. **59**(6): p. 2522-2528.
63. Case, D.A., et al., *AmberTools.* J Chem Inf Model, 2023. **63**(20): p. 6183-6191.
64. Tian, C., et al., *ff19SB: Amino-Acid-Specific Protein Backbone Parameters Trained against Quantum Mechanics Energy Surfaces in Solution.* J Chem Theory Comput, 2020. **16**(1): p. 528-552.
65. Dickson, C.J., R.C. Walker, and I.R. Gould, *Lipid21: Complex Lipid Membrane Simulations with AMBER.* J Chem Theory Comput, 2022. **18**(3): p. 1726-1736.
66. Meagher, K.L., L.T. Redman, and H.A. Carlson, *Development of polyphosphate parameters for use with the AMBER force field.* J Comput Chem, 2003. **24**(9): p. 1016-25.
67. Allner, O., L. Nilsson, and A. Villa, *Magnesium Ion-Water Coordination and Exchange in Biomolecular Simulations.* J Chem Theory Comput, 2012. **8**(4): p. 1493-502.
68. Salomon-Ferrer, R., et al., *Routine Microsecond Molecular Dynamics Simulations with AMBER on GPUs. 2. Explicit Solvent Particle Mesh Ewald.* J Chem Theory Comput, 2013. **9**(9): p. 3878-88.
69. Roe, D.R. and B.R. Brooks, *A protocol for preparing explicitly solvated systems for stable molecular dynamics simulations.* J Chem Phys, 2020. **153**(5): p. 054123.
70. Quigley, D. and M.I. Probert, *Langevin dynamics in constant pressure extended systems.* J Chem Phys, 2004. **120**(24): p. 11432-41.
71. Harris, J.A., et al., *GPU-Accelerated All-Atom Particle-Mesh Ewald Continuous Constant pH Molecular Dynamics in Amber.* J Chem Theory Comput, 2022. **18**(12): p. 7510-7527.
72. Kräutler, V., W.F. van Gunsteren, and P.H. Hünenberger, *A fast SHAKE algorithm to solve distance constraint equations for small molecules in molecular dynamics simulations.* J. Comput. Chem., 2001. **22**(5): p. 501-508.
73. Roe, D.R. and T.E. Cheatham, 3rd, *PTRAJ and CPPTRAJ: Software for Processing and Analysis of Molecular Dynamics Trajectory Data.* J Chem Theory Comput, 2013. **9**(7): p. 3084-95.
74. Humphrey, W., A. Dalke, and K. Schulten, *VMD: visual molecular dynamics.* J Mol Graph, 1996. **14**(1): p. 33-8, 27-8.
75. Magdziarz, T., et al., *AQUA-DUCT: a ligands tracking tool.* Bioinformatics, 2017. **33**(13): p. 2045-2046.

76. Passaro, S., et al., *Boltz-2: Towards Accurate and Efficient Binding Affinity Prediction.* bioRxiv, 2025: p. 2025.06.14.659707.
77. Abts, A., et al., *Easy and Rapid Purification of Highly Active Nisin.* Int. J. Pept, 2011. **2011**(1): p. 175145.

732 **Tables**

733

734 **Table 1**. Site-directed mutagenesis at the intracellular NisG helix impairs NisFEG function.

	NisFEG control	$NisF_{H118A}$	$NisF_{K129A}$	$NisG_{N72A}$	$NisG_{Q75A}$	$NisE_{Q76A}$
IC_{50} (nM)	118	12	76	93	98	118
F. o. R[1]	10	1	6	8	8	10
Activity (%)	100	0	64	76	83	100

735 [1.] Factor of resistance.

736

737 **Table 2.** Mutagenic primers used in the present study.

Primer	Sequence (5'-3')
NisF_N72A-for	GAGTCTGGCCGCACGTTTCCAAG
NisF_N72A_rev	TCCTGTTCAAAGATTAGAATAG
NisE_Q76A_for	TGGAAATTTTGCAAATGTGAAATGGAAAAAG
NisE_Q76A_rev	GCTTGCTCCTCTGATTTTATATC
NisF_K129A_for	GAAAGAAAAGAGCAGGAAAATTCTCTTTAGGGATGGCGCAACGTTTGG
NisF_K129A_rev	CTGTTTCTGCCAAACCAATCACTTCTAGAGTTTCATGAATTCTCTTATC
NisF-H181A-for	GACAATCTTGATTTCTAGTGCTCAGTTGCACGAAATAAGTAAAG
NisF-H181A-rev	CTTTACTTATTTCGTGCAACTGAGCACTAGAAATCAAGATTGTC
NisG-Q75A_for	GCCAATCGTTTCGCGGAAATAAATG
NisG-Q75A_rev	CAGACTCTCCTGTTCAAAGATTAGAATAGAC

738

739 **Figures**

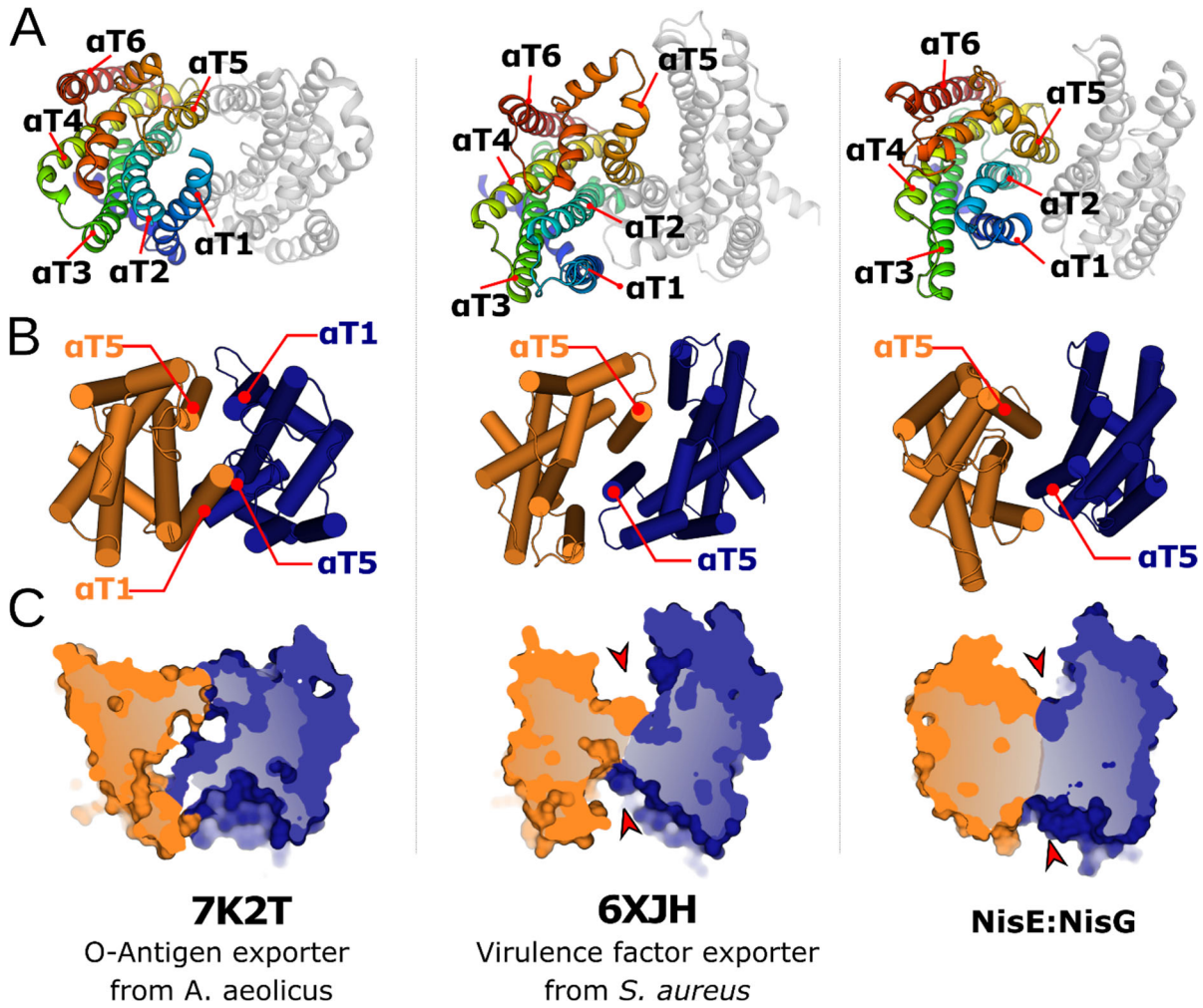

740

741 **Figure 1. Architecture of the transmembrane region of NisFEG.** A) Experimentally
742 determined structures of the the O-antigen transporter Wzm/Wzt from *Aquifex aeolicus* (left;
743 PDB ID 7K2T) and the virulence factor exporter PmtCD from *Staphylococcus aureus* (center;
744 PDB ID 6XJH), and the structural model of NisFEG. For each model, the left chain (identical
745 chains in the case of PmtCD and Wzt, NisE shown for NisFEG) is colored from the N-terminus
746 (blue) to the C-terminus (red) and membrane-spanning helices are labeled from αT1 to αT5. B)
747 For each model, a cylindrical cartoon representation of the transmembrane region is shown
748 highlighting the interfacial helixes. In the case of NisFEG, NisE is colored orange, while NisG
749 is colored blue. C) Perpendicular cross-section of each complex. Pronounced clefts are
750 highlighted with red arrowheads. The same coloring scheme applies as in B).

751

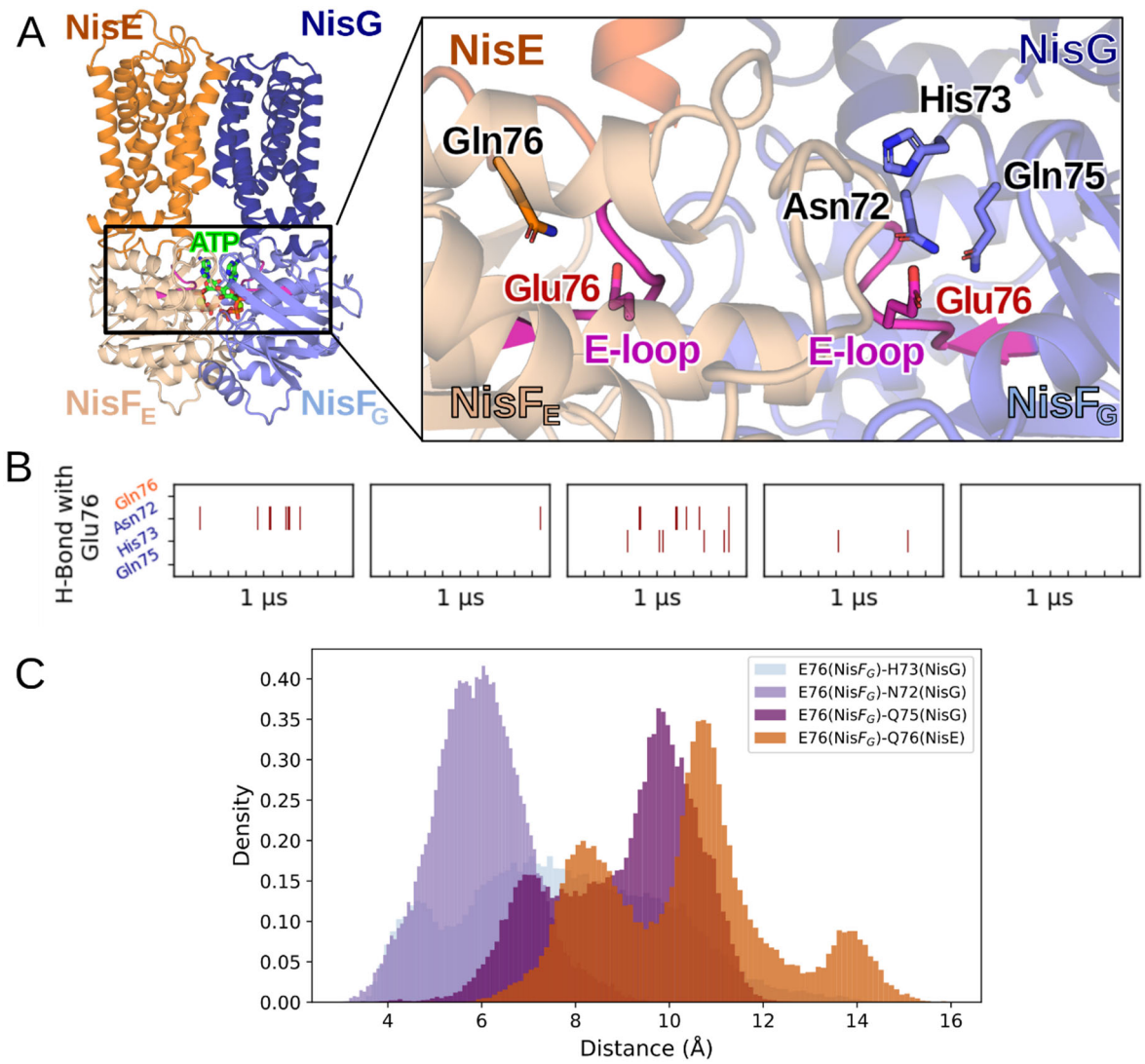

Figure 2. The E-loop mediates interactions with the transmembrane chains of NisFEG. A) Global view of the NisFEG complex model, with the E-loop of both NisF chains highlighted in pink and the ATP molecules shown as green sticks. The right panel shows a close-up of the E-loop. The surrounding residues are shown as sticks and labeled accordingly. B) Time-series showing the presence of hydrogen bonds between Glu76 of the E-loop in $NisF_G$ (marked in blue at the Y-axis) and $NisF_E$ (marked in orange at the Y-axis). The red stripes represent when the residue pairs are forming an effective hydrogen bond (distance < 3.5 Å between hydrogen and the acceptor and angle > 135° for acceptor-hydrogen-donor) across each replica. C) Histograms showing the pairwise distance distribution between Glu76 and its possible interacting partners across the aggregated simulation time; color code as in panel B.

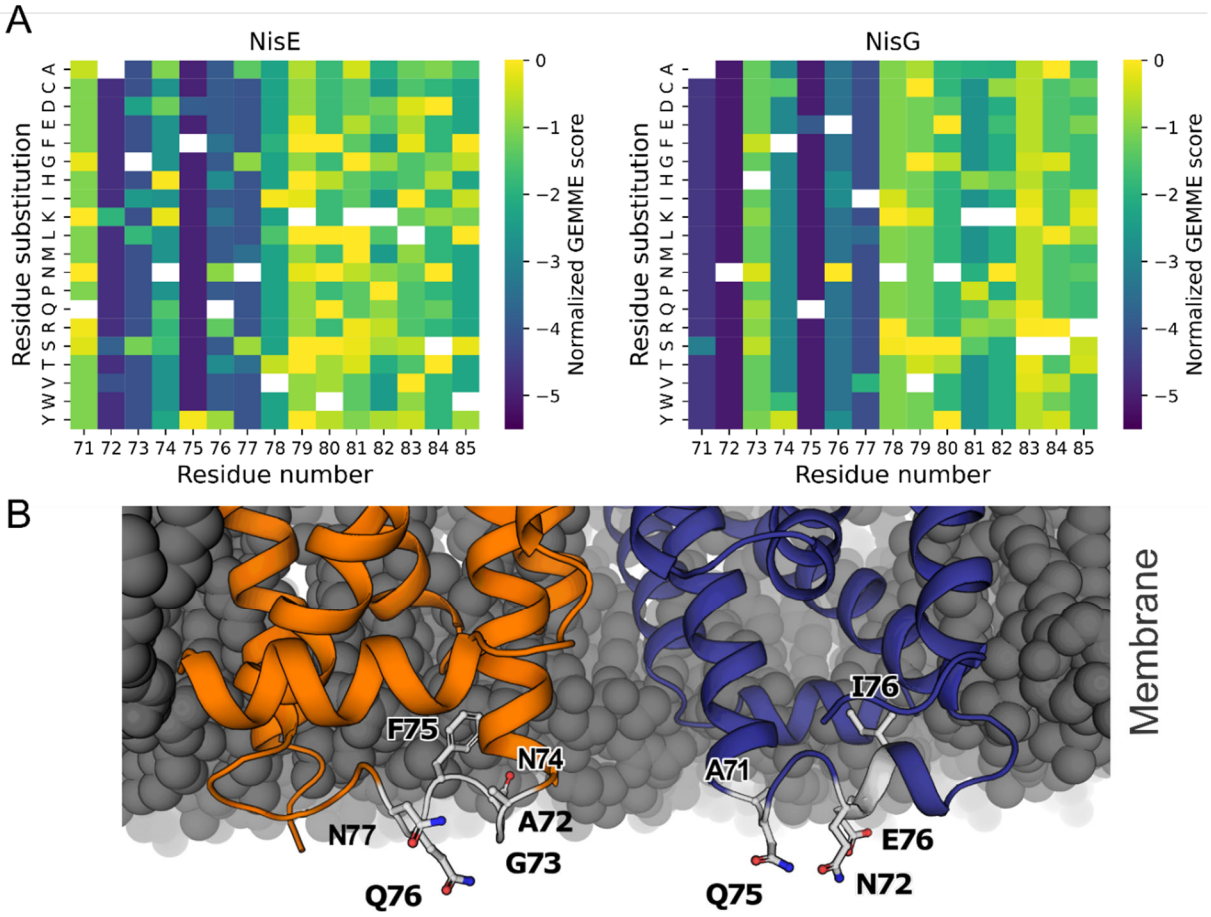

Figure 3. Solvent-exposed residues on the intracellular helix of NisG are more conserved, and their loss could lead to functional disruption. A) GEMME score for residues belonging to NisE intracellular helix. Lower scores indicate a higher degree of conservation and, therefore, a higher likelihood of a residue being functionally relevant. B) Cross-section view of the inner leaflet of the membrane, showing the intracellular section of NisE (orange) and NisG (blue). Residues with low GEMME scores belonging to the intracellular helices are highlighted as sticks -

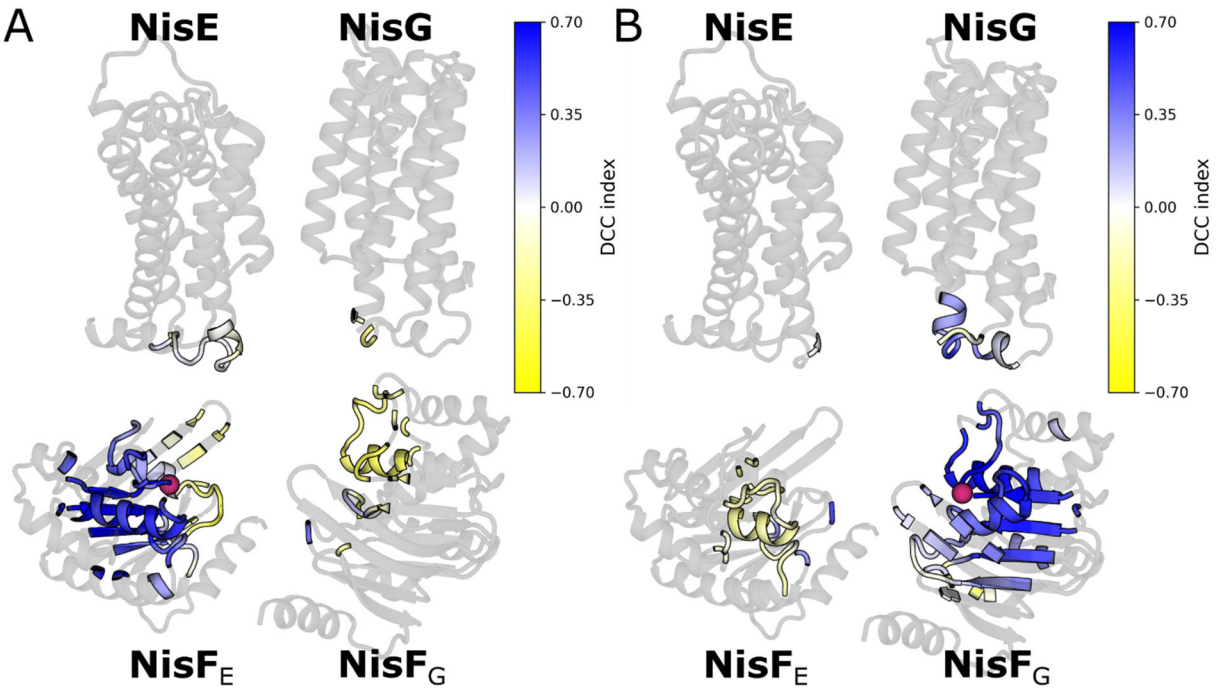

Figure 4. Movements of the E-loop are correlated to those in NisG but not in NisE. A) View of each individual chain of NisFEG. Residues within a radius of 15 Å of the central E-loop residue Glu76 (C_α atom highlighted as orange sphere) are colored according to their dynamic cross correlation (DCC) index. The dark blue regions are those moving colinearly with Glu76. B) Same as in A, but highlighting the residues surrounding Glu76 in the E-loop of the second NisF subunit. The same color scale applies to both panels.

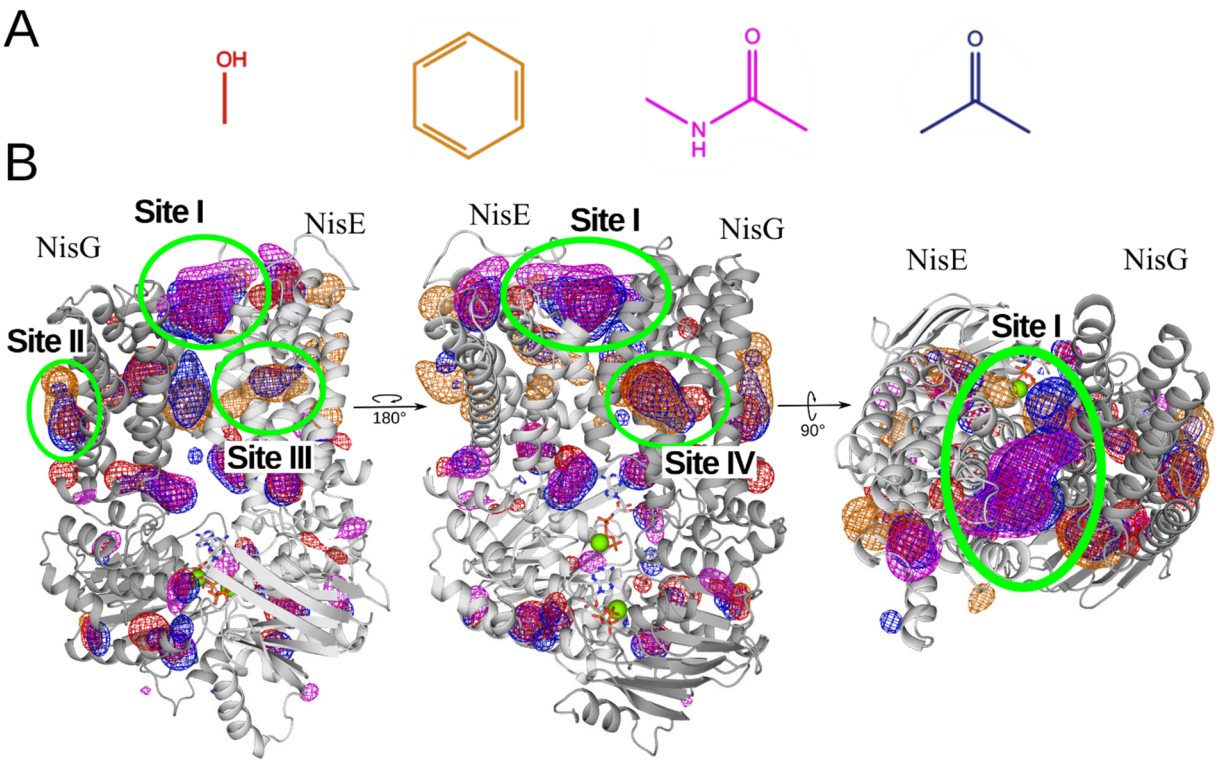

780

Figure 5. Cosolvent MD simulations reveal putative nisin interaction sites. A) Structure of the used cosolvent probes. Red: Methanol. Orange: Benzene. Magenta: *N*-Methylacetamide Blue: Acetone. B) Density map of the cosolvent probes across the NisFEG complex. Larger densities are observed within the transmembrane region of the transporter. Regions where three or more probes accumulate are highlighted with a green circle and labeled. There are four main sites: one located at the extracellular side of the transporter, at the interface between NisE and NisG (site I), another at the periphery of NisG (site II), and two sites in the transmembrane clefts, one in NisE (site III) and one in NisG (site IV).

781

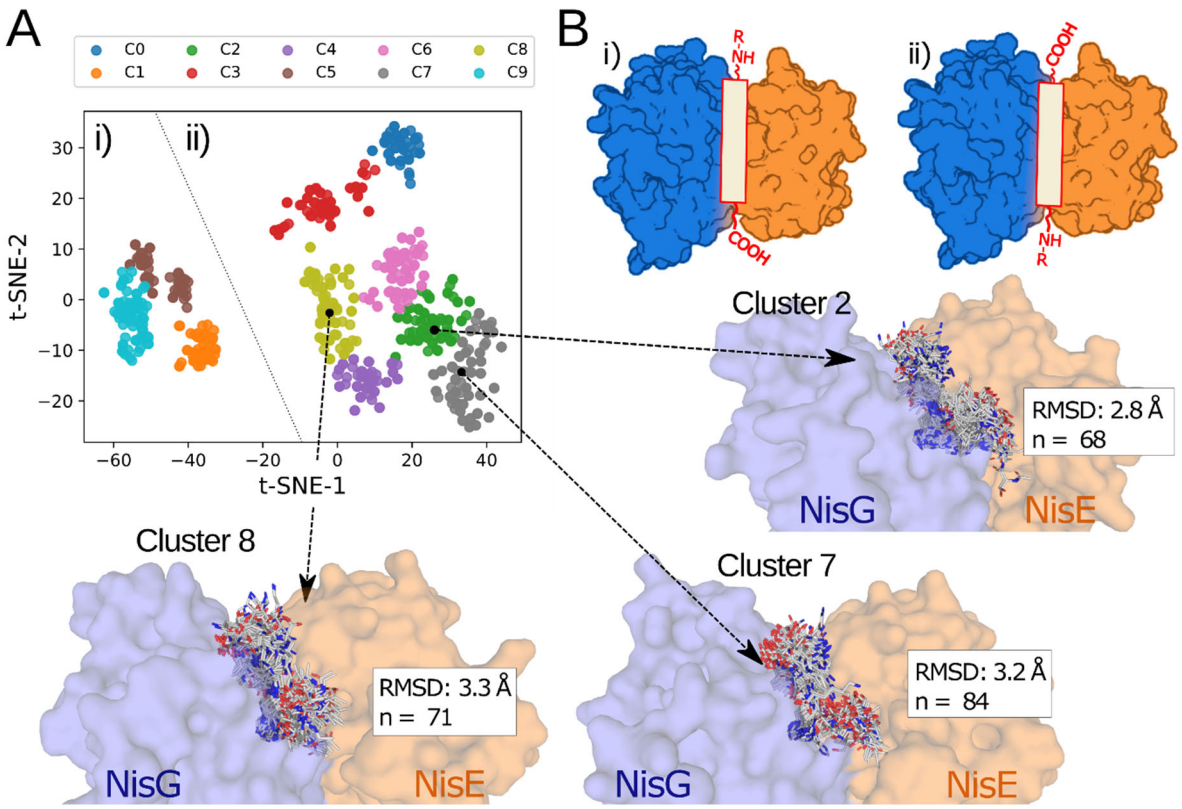

Figure 6. Boltz-2 sampling of C-Nis shows a putative binding site on the extracellular cleft between NisE:NisG. A) t-distributed Stochastic Neighbor Embedding projection derived from the coordinates of the C-Nis atoms when co-modelled with NisFEG. The data is split into two large clusters, labeled i) and ii). The datapoints are colored according to subclusters identified by GMM. Dashed arrow lines point to the ensemble of structures belonging to the three largest sub-clusters. B) Schematic representation of the two possible orientations of C-Nis corresponding to each one of the main clusters (i) and ii) in panel A.

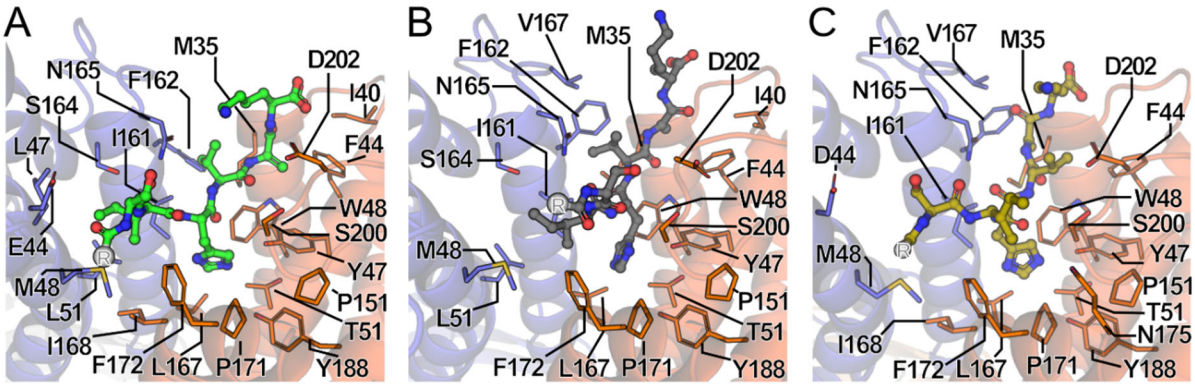

Figure 7. Binding mode of C-Nis derived from the representative poses of the main clusters. Residues within 5 Å of C-Nis in NisG (blue) and NisE (orange) for each one of the largest sub-clusters shown in Figure 6A. The cap atom is highlighted as a gray sphere labeled "R". A) Subcluster 2, C-Nis shown as green sticks. B) Subcluster 7, C-Nis shown as gray sticks. C) Subcluster 8, C-Nis shown as olive sticks.

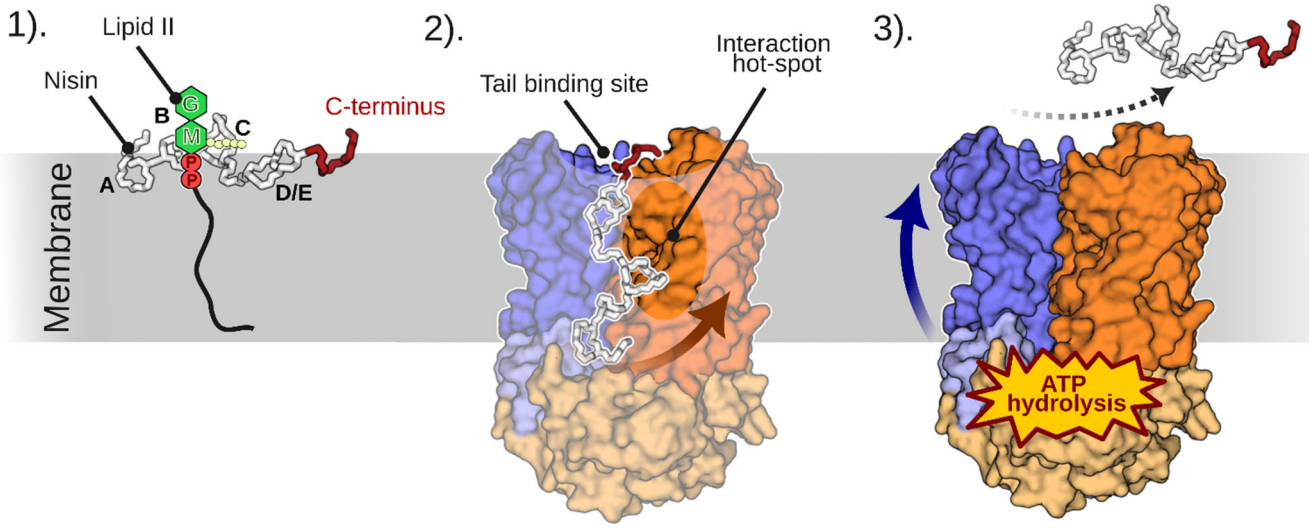

Figure 8. Scheme of a hypothetical mechanism of action for NisFEG. 1) Nisin is bound to Lipid II, but the formation of larger oligomers that form bacteriolytic pores has not yet taken place, therefore, the D/E rings and the C-terminus of nisin move freely. 2) Nisin is first recognized by NisFEG via an interaction of the C-terminus of nisin with the binding sites on NisE (orange arrow). 3) An ATP-powered conformational rearrangement orchestrated by contacts between the E-loop and NisG drives the extrusion of nisin to the extracellular medium (blue arrow), freeing Lipid II and preventing the formation of pores.